Intermetallics 95 (2018) 80–84

Contents lists available at ScienceDirect

Intermetallics

journal homepage: www.elsevier.com/locate/intermet

Mapping the magnetic transition temperatures for medium- and high-entropy alloys

Shuo Huang[a,*], Erik Holmström[b], Olle Eriksson[c,d], Levente Vitos[a,c,e,**]

[a] Applied Materials Physics, Department of Materials Science and Engineering, Royal Institute of Technology, Stockholm, SE-100 44, Sweden
[b] Sandvik Coromant R&D, 126 80, Stockholm, Sweden
[c] Department of Physics and Astronomy, Division of Materials Theory, Uppsala University, Box 516, SE-75120, Uppsala, Sweden
[d] School of Science and Technology, Örebro University, SE-701 82, Örebro, Sweden
[e] Institute for Solid State Physics and Optics, Wigner Research Centre for Physics, P.O. Box 49, H-1525, Budapest, Hungary

ARTICLE INFO

Keywords:
Curie temperature
High-entropy alloys
First-principle calculations
Monte-Carlo simulations

ABSTRACT

Tailorable magnetic state near room temperature is very promising for several technological, including magnetocaloric applications. Here using first-principle alloy theory, we determine the Curie temperature (T_C) of a number of equiatomic medium- and high-entropy alloys with solid solution phases. All calculations are performed at the computed lattice parameters, which are in line with the available experimental data. Theory predicts a large crystal structure dependence of T_C, which explains the experimental observations under specified conditions. The sensitivity of the magnetic state to the crystal lattice is reflected by the magnetic exchange interactions entering the Heisenberg Hamiltonian. The analysis of the effect of composition on T_C allows researchers to explore chemistry-dependent trends and design new multi-component alloys with pre-assigned magnetic properties.

1. Introduction

Based on a distinct concept of alloy design, Yeh et al. introduced a new class of materials, the high-entropy alloys (HEAs) [1], which has attracted extensive attention from the academic and metallurgic research communities over the recent years [2–6]. Unlike conventional alloys, HEAs are characterized by their special compositions containing multiple elements in equal or near-equal molar ratios. Several important features in these alloys have been postulated, including high entropy, sluggish diffusion, and severe lattice distortion [7]. It is of particular interest to notice that many reported HEAs possess simple [e.g., face-centered cubic (fcc) and/or body-centered cubic (bcc) structures] yet chemically disordered solid solution phases [8]. In addition, these alloys display a variety of technologically appealing and tunable properties, such as excellent specific strength [9], exceptional ductility and fracture toughness at cryogenic temperatures [10], encouraging fatigue resistance [11], and superconductivity [12].

Recently, it was suggested that HEAs could be exciting candidate materials for magnetic refrigeration applications. The key parameters in focus are the magnetic entropy change, the adiabatic temperature change and the refrigerant capacity [13]. Belyea et al. found that NiFeCoCrPd$_x$ displays a second order magnetic phase transition associated with a slightly decreasing magnetic entropy change and increasing critical temperature from ~100 K to room temperature, which leads to nearly 40% enhancement of the refrigerant capacity as x increases from null to 11.11% [14]. Yuan et al. showed that GdDyErHoTb exhibits the largest refrigerant capacity reported so far (~627 J kg^{-1} at the 5 T magnetic field), along with a small magnetic hysteresis loss and ductile mechanical behavior [15]. In most cases, the refrigeration parameters can be maximized near the critical temperature and thus for widespread applications the magnetocaloric material should possess Curie temperature (T_C) close to the room temperature.

Previous work indicate that T_C of HEAs is sensitive to the base composition, the additional alloying elements, and the crystal structure [16,17]. In the widely-studied FeCrCoNiAl$_x$ system, for example, Al addition increases the T_C from 130 K for FeCrCoNi to 430 K for FeCrCoNiAl$_2$ [18–20], associated with a structural transition from fcc to bcc with an fcc-bcc duplex region [21–23]. On the other hand, the available experimental critical temperatures often carry an unknown error bar due to the difficulties associated with synthesizing homogeneous solid solutions [18,19,21]. Despite the appreciable efforts in experiments, very little theoretical investigations devoted to this question have been presented so far. This can be attributed to the complexity of the problem related to the magnetic and chemical disorder in connection with

* Corresponding author.
** Corresponding author. Applied Materials Physics, Department of Materials Science and Engineering, Royal Institute of Technology, Stockholm, SE-100 44, Sweden.
E-mail addresses: shuoh@kth.se (S. Huang), levente@kth.se (L. Vitos).

https://doi.org/10.1016/j.intermet.2018.01.016
Received 30 November 2017; Received in revised form 12 January 2018; Accepted 20 January 2018

Table 1
List of equiatomic medium- and high-entropy alloys crystallizing in the fcc and/or bcc phases. The calculated equilibrium Wigner-Seitz radius in ferromagnetic (paramagnetic) state and Curie temperature are presented, along with the available experimental and other theoretical data.

Alloy	Phases	Wigner-Seitz radius (bohr)				Curie temperature (K)		
		fcc	Expt.	bcc	Expt.	fcc	Expt./Cal.	bcc
AlNiCu	fcc + bcc [34]	2.711	2.690 [34]	2.710	2.767 [34]	–		–
CrFeNi	fcc [35]	2.626 (2.619)		2.636 (2.632)		80		225
CrCoNi	fcc [36]	2.609 (2.604)	2.636 [36]	2.622 (2.618)		25		120
MnFeNi	fcc [35]	2.617 (2.624)		2.646 (2.652)		43		71
FeCoNi	fcc [37]	2.629 (2.606)	2.658 [37]	2.635 (2.624)		804	995 [38]	1147
AlFeCoNi	bcc [37]	2.668 (2.654)		2.669 (2.663)	2.682 [37]	497		763
AlCoNiCu	fcc + bcc [34]	2.674 (2.670)	2.661 [34]	2.676 (2.674)	2.737 [34]	197		245
VCrFeMo	bcc [39]	2.790 (2.789)		2.771 (2.769)		21		251
CrFeCoNi	fcc [21]	2.619 (2.604)	2.644 [21]	2.630 (2.624)		155	120–130 [16,18,20]	414
MnFeCoNi	fcc [40]	2.616 (2.606)	2.657 [40]	2.655 (2.640)		166		580
FeCoNiCu	fcc [41]	2.641 (2.632)	2.648 [41]	2.647 (2.642)		796	826 [26]	987
AlTiFeNiCu	fcc + bcc [42]	2.767 (2.765)		2.762 (2.760)		213		286
AlCrMnFeCo	bcc [43]	2.667 (2.660)		2.670 (2.658)	2.680 [43]	32		463
AlCrFeCoNi	fcc + bcc [21]	2.661 (2.653)	2.667 [21]	2.664 (2.659)	2.683 [21]	136		334
AlCrFeNiCu	fcc + bcc [44]	2.689 (2.688)		2.686 (2.683)		124		159
AlCrCoNiCu	fcc + bcc [34]	2.671 (2.671)	2.650 [34]	2.673 (2.671)	2.726 [34]	25		70
AlFeCoNiCu	fcc + bcc [45]	2.672 (2.665)	2.670 [45]	2.674 (2.670)	2.668 [45]	493		663
TiVCrFeMo	bcc [39]	2.836 (2.835)		2.799 (2.794)		31		97
TiCrFeCoNi	fcc [46]	2.690 (2.682)		2.691 (2.684)		95		339
VMnFeCoNi	fcc [47]	2.638 (2.636)		2.664 (2.652)		27		470
VFeCoNiCu	fcc [48]	2.662 (2.652)		2.666 (2.661)		246		404
CrMnFeCoNi	fcc [49]	2.607 (2.604)	2.659 [49]	2.640 (2.630)		27	20 [50]	397
CrMnFeCoCu	fcc [47]	2.647 (2.630)		2.656 (2.647)		59		477
CrMnFeNiCu	fcc + bcc [44]	2.664 (2.647)		2.664 (2.655)		60		191
CrFeCoNiCu	fcc [1]	2.638 (2.626)	2.642 [1]	2.643 (2.638)		251	172 [51]	382
CrFeCoNiPd	fcc [19]	2.716 (2.706)	2.694 [19]	2.717 (2.723)		440	440 [19]	414
CrFeNiCuMo	fcc [44]	2.743 (2.740)		2.740 (2.739)		102		144
MnFeCoNiCu	fcc [52]	2.646 (2.643)		2.671 (2.657)		146	400 [52]	540
MnFeCoNiGa	fcc + bcc [40]	2.676 (2.673)	2.715 [40]	2.695 (2.685)	2.654 [40]	77		567
MnFeCoNiMo	fcc [47]	2.721 (2.717)		2.735 (2.731)		68		540
FeCoNiCuMo	fcc [52]	2.731 (2.726)		2.736 (2.733)		328	657 [52]	508
FeCoNiCuAg	fcc [52]	2.752 (2.750)		2.757 (2.756)		805		881
FeCoNiCuPt	fcc [52]	2.748 (2.745)		2.757 (2.755)		837	864 [52]	879
AlSiFeCoNiCu	fcc + bcc [45]	2.673 (2.666)	2.693 [45]	2.677 (2.672)	2.638 [45]	281		438
AlTiCrFeCoNi	fcc + bcc [46]	2.721 (2.716)		2.718 (2.715)		93		264
AlTiFeCoNiCu	fcc + bcc [45]	2.730 (2.724)	2.681 [45]	2.729 (2.723)	2.709 [45]	274		438
AlCrFeCoNiCu	fcc + bcc [45]	2.669 (2.661)	2.669 [45]	2.670 (2.665)	2.671 [45]	176		300
TiCrMnFeCoNi	fcc + bcc [53]	2.686 (2.677)	2.688 [53]	2.687 (2.678)		37		380
VCrMnFeCoNi	fcc [53]	2.637 (2.637)	2.644 [53]	2.654 (2.645)		10		288
CrMnFeCoNiCu	fcc [53]	2.652 (2.630)	2.651 [53]	2.656 (2.646)		124		371
CrMnFeCoNiGe	fcc + bcc [53]	2.679 (2.663)	2.644 [53]	2.682 (2.676)		97		346
AlSiCrFeCoNiCu	fcc + bcc [34]	2.670 (2.664)	2.647 [34]	2.672 (2.668)	2.723 [34]	104		213

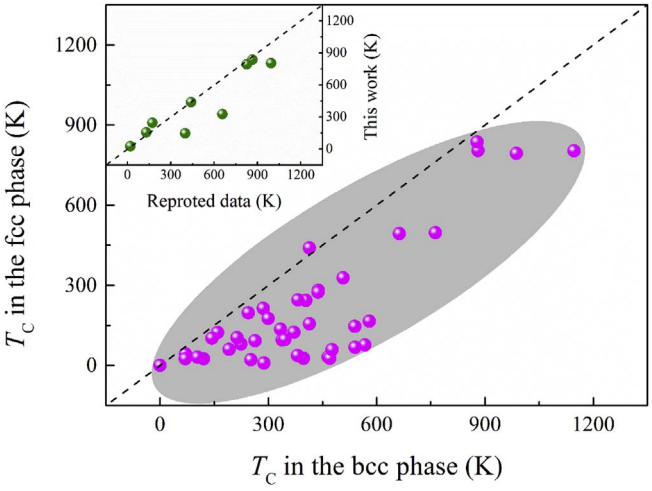

Fig. 1. Theoretical Curie temperatures (T_C) calculated in the bcc and fcc phases for systems listed in Table 1. The inset shows the comparison of T_C between our results and the available experimental and theoretical data for system in the fcc phase.

the multicomponent nature of the HEAs. In order to foster an intelligent T_C tailoring in promising magnetocaloric and other magnetic high-entropy alloys, here we put forward a systematic theoretical investigation for a large number of equiatomic system with solid solution phases.

2. Theoretic methods

The Heisenberg model [24], in combination with the *ab initio* exchange interaction parameters and Monte-Carlo simulations, can provide accurate magnetic transition temperatures for magnetic alloys including high-entropy alloys [17]. Alternatively, one can employ the mean-field approximation (MFA) and evaluate T_C from the *ab initio* energies according to $3k_B T_C = 2(E_{PM} - E_{FM})/(1 - c)$, where k_B is the Boltzmann constant, c is the concentration of the nonmagnetic component, and E_{PM} and E_{FM} are the equilibrium total energies per atom for the paramagnetic (PM) and ferromagnetic (FM) states, respectively. The MFA was found to have the necessary accuracy and predictive power to reveal the magnetic properties for diluted magnetic semiconductors [25], as well as some HEAs [26]. Considering the documented success and high efficiency of the MFA, here we carry out the T_C mapping of a large number of HEAs using this approach. However, we discuss and assess the MFA results for a few particular cases using the more elaborated Heisenberg model. The total energy and exchange interaction

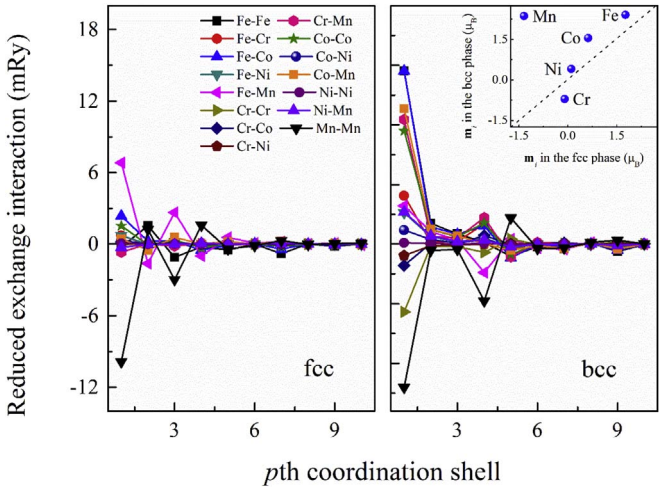

Fig. 2. The magnetic exchange interactions for different pair atoms in CrMnFeCoNi as a function of *p*th coordination shell. The inset shows the magnetic moments of each components for the fcc and bcc phases, respectively.

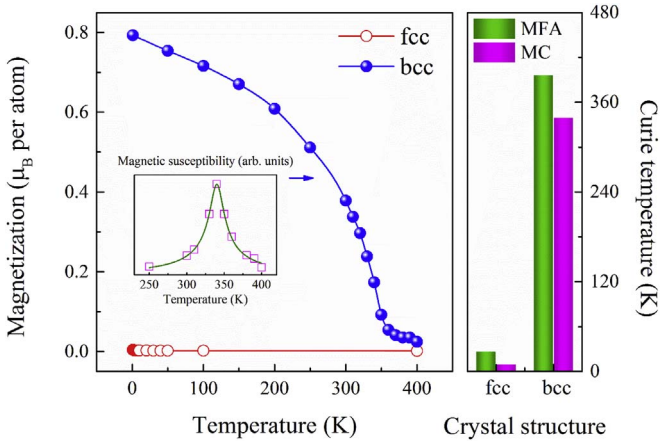

Fig. 3. Left panel: Theoretical magnetization versus temperature for CrMnFeCoNi in the fcc and bcc phases, respectively. The inset shows the magnetic susceptibility in the bcc phase. Results are obtained using Monte-Carlo (MC) simulations based on Heisenberg Hamiltonian and *ab initio* exchange interaction parameters. Right panel: Comparison of Curie temperature obtained via MFA and MC approaches for CrMnFeCoNi in the fcc and bcc phases, respectively.

calculations were carried out using density functional theory implemented in the framework of the exact muffin-tin orbital (EMTO) formalism [27,28]. The chemical and magnetic disorders in random system were treated within the coherent potential approximation (CPA) [29–31]. The exchange-correlation effects were taken into account within the generalized gradient approximation in the form of Perdew, Burke and Ernzerhof (PBE) [32]. The one-electron Kohn-Sham equations were solved within the scalar-relativistic approximation and soft-core scheme. The paramagnetic state was simulated by the disordered local moments (DLM) approximation [33]. All calculations were performed for completely disordered solid solution and static lattice.

3. Results and discussion

Table 1 shows the basic properties of the selected equiatomic medium- and high-entropy alloys, including crystal structure, Wigner-Seitz radius, and Curie temperature. The majority of the selected alloys are based on the late 3*d* transition metals [1,18–21,26,34–53]. Considering the fact that many of the present alloys, especially the Al containing systems, possess a mixture of the fcc and bcc phases, in Table 1 we give the theoretical results for these two phases to bring to light the related properties as a function of crystal structure.

In Table 1, we compare the theoretical Wigner-Seitz radius with the corresponding values converted from the available experimental lattice parameters. It is found that the two sets of data are in reasonable agreement with each other, and the relative deviation between theory and experiment is below ~2.5%. At the same time, in Fig. 1 (inset), we plot the calculated T_C with reported values for some systems. As can be seen, the present theoretical work reproduces the trend shown in other studies, confirming the predictive power of our MFA-based approach.

To illustrate and explore the alloying trends of the studied properties, here we take FeCoNiCu (in the fcc phase) as a base alloy, and consider the equimolar V, Cr, Mn, Mo, Ag, and Pt additions. As shown in Table 1, the calculated equilibrium Wigner-Seitz radius for FeCoNiCu in ferromagnetic state is 2.641 bohr, which agrees well with the corresponding experimental value of 2.648 bohr [41]. Alloying with Cr decreases the volume of the FeCoNiCu host, in line with the experimental observation [1,41]. In contrast, a volume increases is predicted when adding V, Mn, Mo, Ag, and Pt, which should partially be attributed by the larger atomic radius of the considered elements as compared to that of Cr [54].

The calculated T_C for FeCoNiCu is 796 K, which compares well with the previous theoretical value of 826 K [26]. A significant decrease in the T_C is revealed when adding equimolar V, Cr, and Mn to the host

Table 2
Prediction of Wigner-Seitz radius and Curie temperature for some equiatomic medium- and high-entropy alloys in the bcc phase. The columns denoted as "average" list values obtained according to Vegard's law based on the experimental Wigner-Seitz radii of the alloy components.

Alloy	Wigner-Seitz radius (bohr)		Curie temperature (K)	Alloy	Wigner-Seitz radius (bohr)		Curie temperature (K)
	EMTO-CPA	average			EMTO-CPA	average	
AlVCr	2.775	2.829	–	AlVCrMn	2.717	2.797	–
AlVMn	2.742	2.835	–	AlVCrFe	2.723 (2.716)	2.789	119
AlVFe	2.756 (2.747)	2.824	292	AlVMnFe	2.708 (2.701)	2.793	190
AlCrMn	2.690	2.792	–	AlVNbMo	2.947	2.951	–
AlCrFe	2.704 (2.699)	2.781	288	AlVNbW	2.959	2.953	–
TiVNb	2.972	2.979	–	AlCrMnFe	2.672 (2.667)	2.760	189
TiVMo	2.909	2.931	–	TiVCrMn	2.741	2.812	–
TiCrMo	2.866	2.888	–	TiVCrMo	2.848	2.870	–
TiNbMo	3.003	3.017	–	TiVNbMo	2.956	2.966	–
VCrMn	2.668	2.732	–	VCrMnFe	2.660 (2.656)	2.716	221
VCrFe	2.678 (2.672)	2.721	253	VCrNbMo	2.881	2.874	–
VMnFe	2.666 (2.658)	2.727	395	AlTiVCrMn	2.776	2.848	–
VNbMo	2.943	2.937	–	AlVCrMnFe	2.692 (2.688)	2.771	102
AlTiVMn	2.813	2.889	–	AlVCrNbW	2.905	2.899	–
AlTiVFe	2.821 (2.811)	2.881	181	AlVCrNbMoW	2.911	2.904	–
AlTiCrMn	2.773	2.857	–				

composition. The main reason for this decrease is the appearance of the antiferromagnetic coupling between V/Cr/Mn moments and the Fe-Co-Ni matrix, as demonstrated below in the case of CrMnFeCoNi, and some other systems [17,20,55]. On the other hand, the addition of noble metals, i.e., Ag and Pt, is found to slightly increase the T_C of the host alloy. It is of particular interest that in experiment, equimolar Pd addition to CrFeCoNi increases the T_C from 130 K to 440 K [18,19]. Our data indicates a very similar trend for Pt-doped FeCoNiCu. From this point of view, alloying with noble metals is expected to be a promising route for fine T_C tuning.

For system with fcc-bcc duplex phases considered here, T_C is predicted to be larger in the bcc phase than in the fcc phase. Actually this trend is consistent with the previous work addressing the crystal structure dependence of the magnetic behavior for $CrFeCoNiAl_x$ HEAs [17]. Indeed, as shown in Fig. 1, the above crystal structure effect is found for most of the systems considered in this work. Here we would like to highlight a particularly interesting experimental fact which now gains theoretical support in the mirror of the present data. It is known that unusual properties can occur in HEAs when specified manufacturing process is employed. The single-phase equiatomic CrMnFeCoNi alloy [53], which crystallizes in an fcc lattice, is one of the well-studied examples. Experimental measurements indicate that the system is in a paramagnetic state down to a temperature of 93 K (i.e., the magnetic transition temperature should be below 93 K) [56]. However, during mechanical alloying and spark plasma sintering process, in the fcc solid solution matrix a minority bcc phase formed. Measuring the magnetic hysteresis curves of these two-phase alloys at room temperature indicated that the as-milled powder possesses the characteristic feature of soft magnet [57], which is fully supported by the presently predicted T_C for the bcc phase.

To understand the magnetic characteristics of CrMnFeCoNi and the strong crystal structure dependence, here we investigate the magnetic exchange interactions between alloy components. Fig. 2 shows the reduced parameter $J'_{ij} = z_p J_{ij} \boldsymbol{m}_i \boldsymbol{m}_j$, where i and j are atomic indices, $\mathbf{m}_i$ is the magnetic moment, J_{ij} is the strength of the exchange interaction, and z_p is the coordination number of the pth coordination shell. As indicated from Fig. 2, the dominating ferromagnetic interactions in the bcc phase are between the nearest-neighbor Fe-Fe, Fe-Co, Co-Co, and Co-Mn pairs, and the anti-ferromagnetic interactions between the nearest-neighbor Cr-Cr, Cr-Mn, and Mn-Mn pairs. We mention that Cr is anti-parallel with Mn (as shown in the inset of Fig. 2), thus the positive value of exchange parameter between Cr and Mn indicates an anti-ferromagnetic coupling. In the case of the fcc phase, the magnetic behavior is mainly due the anti-ferromagnetic couplings between Fe-Mn and Mn-Mn at the nearest-neighbor distance. Hence, one would expect a weaker magnetic ordering tendency and a lower critical temperature for the fcc alloys compared to those for the bcc phase.

Using the present exchange interaction parameters in the Heisenberg Hamiltonian, we performed Monte-Carlo simulations for both fcc and bcc lattices [17,58]. Fig. 3 shows the temperature dependent magnetization and magnetic susceptibility. It is found that the T_C of CrMnFeCoNi is 10 ± 10 K for the fcc phase and 340 ± 10 K for the bcc phase. We recall that the T_C calculated via MFA for this system in the fcc and bcc phases are 27 K and 397 K, respectively. The good agreement between these two approaches gives a strong support for our T_C maps presented in Table 1 (also Table 2). We emphasize the large structural factor for the T_C. Besides explaining the experimental observation, the strong structure dependence of the magnetic order opens new opportunities for further magnetocaloric applications.

Senkov et al. evaluated thousands of equimolar alloy compositions for potential high-temperature applications by combining calculated phase diagrams with simple empirical rules [59]. Based on that work, we expand our study to some promising candidate compositions, as listed in Table 2, which are suggested to possess single bcc phase at 873 K. Taking AlVCrNbMoW as an example, the Wigner-Seize radius is 2.904 bohr as determined from Vegard's rule using the experimental volumes of the alloy components [28,60]. This estimated value is close to the EMTO-CPA result of 2.911 bohr. The detailed comparison of the two sets of data is presented in Table 2. As can be seen, there is a general good agreement between these two theoretical predictions.

To provide insight for selecting possible magnetic materials, T_C is also shown in Table 2. It is immediately clear that many of the selected system are nonmagnetic, while others, e.g., the Fe containing systems, show relatively low T_C. This is not surprising as most of them contain a large amount of nonmagnetic elements such as Al, Ti, Nb, Mo, and W, which dilutes the ferromagnetic component of Fe. We notice that the present data can be used as a guide to adjust the alloy compositions to a target T_C. For example, the predicted T_C for VMnFe and VCrMnFe are 395 K and 221 K, respectively. From linear combination we get 308 K for $VCr_{0.5}MnFe$, which is surprisingly close to 292 K obtained from direct MFA calculation. In addition, high T_C is expected for low Cr concentration, which is line with the experimental observation for $Cr_xFeCoNi$ system [18].

4. Conclusions

In summary, we put forward a systematic study of the Curie temperature for a number of equiatomic medium- and high-entropy alloys using first-principle theory. Solid solution phases with fcc and/or bcc underlying lattices are considered. Our results are in line with the available theoretical and experimental data. The analysis of alloying addition on the Curie temperature, as well as the application of linear rule of mixture employing base HEAs, are helpful to identify promising magnetic compositions. Furthermore, the fact that certain HEAs have drastically different ordering temperature for the bcc and fcc crystal structures, offers a way to identify alloys with a very sharp change in the magnetic properties close to a structural phase transition. Exploring various means to tune this coupled structural-magnetic transition to the desired temperature range will open new ways for designing materials with great potential in magnetic refrigeration applications.

Acknowledgements

Work supported by the Swedish Research Council, the Swedish Foundation for Strategic Research, the Swedish Foundation for International Cooperation in Research and Higher Education, the Carl Tryggers Foundation, the Sweden's Innovation Agency (VINNOVA Grant No. 2014-03374), the Swedish Energy Agency, the China Scholarship Council, and the Hungarian Scientific Research Fund (OTKA 109570). We acknowledge the Swedish National Supercomputer Centre in Linköping and Stockholm for computer resources.

References

[1] J.W. Yeh, S.K. Chen, S.J. Lin, J.Y. Gan, T.S. Chin, T.T. Shun, C.H. Tsau, S.Y. Chang, Nanostructured high-entropy alloys with multiple principal elements: novel alloy design concepts and outcomes, Adv. Eng. Mater. 6 (2004) 299–303.
[2] Y. Zhang, T.T. Zuo, Z. Tang, M.C. Gao, K.A. Dahmen, P.K. Liaw, Z.P. Lu, Microstructures and properties of high-entropy alloys, Prog. Mater. Sci. 61 (2014) 1–93.
[3] Y.F. Ye, Q. Wang, J. Lu, C.T. Liu, Y. Yang, High-entropy alloy: challenges and prospects, Mater. Today 19 (2016) 349–362.
[4] D.B. Miracle, O.N. Senkov, A critical review of high entropy alloys and related concepts, Acta Mater. 122 (2017) 448–511.
[5] Y. Dong, K. Zhou, Y. Lu, X. Gao, T. Wang, T. Li, Effect of vanadium addition on the microstructure and properties of AlCoCrFeNi high entropy alloy, Mater. Des. 57 (2014) 67–72.
[6] Y.J. Zhao, J.W. Qiao, S.G. Ma, M.C. Gao, H.J. Yang, M.W. Chen, Y. Zhang, A hexagonal close-packed high-entropy alloy: the effect of entropy, Mater. Des. 96 (2016) 10–15.
[7] M.H. Tsai, J.W. Yeh, High-entropy alloys: a critical review, Mater. Res. Lett. 2 (2014) 107–123.
[8] M.C. Gao, J.W. Yeh, P.K. Liaw, Y. Zhang, High-entropy Alloys: Fundamentals and Applications, Springer, Switzerland, 2016.
[9] O.N. Senkov, G.B. Wilks, D.B. Miracle, C.P. Chuang, P.K. Liaw, Refractory high-entropy alloys, Intermetallics 18 (2010) 1758–1765.
[10] B. Gludovatz, A. Hohenwarter, D. Catoor, E.H. Chang, E.P. George, R.O. Ritchie, A

fracture-resistant high-entropy alloy for cryogenic applications, Science 345 (2014) 1153–1158.
[11] M.A. Hemphill, T. Yuan, G.Y. Wang, J.W. Yeh, C.W. Tsai, A. Chuang, P.K. Liaw, Fatigue behavior of $Al_{0.5}$CoCrCuFeNi high entropy alloys, Acta Mater. 60 (2012) 5723–5734.
[12] P. Koželj, S. Vrtnik, A. Jelen, S. Jazbec, Z. Jagličić, S. Maiti, M. Feuerbacher, W. Steurer, J. Dolinšek, Discovery of a superconducting high-entropy alloy, Phys. Rev. Lett. 113 (2014) 107001.
[13] K.A. Gschneidner Jr., V.K. Pecharsky, A.O. Tsokol, Recent developments in magnetocaloric materials, Rep. Prog. Phys. 68 (2005) 1479.
[14] D.D. Belyea, M.S. Lucas, E. Michel, J. Horwath, C.W. Miller, Tunable magnetocaloric effect in transition metal alloys, Sci. Rep. 5 (2015) 15755.
[15] Y. Yuan, Y. Wu, X. Tong, H. Zhang, H. Wang, X.J. Liu, L. Ma, H.L. Suo, Z.P. Lu, Rare-earth high-entropy alloys with giant magnetocaloric effect, Acta Mater. 125 (2017) 481–489.
[16] Y.F. Kao, S.K. Chen, T.J. Chen, P.C. Chu, J.W. Yeh, S.J. Lin, Electrical, magnetic, and Hall properties of AlxCoCrFeNi high-entropy alloys, J. Alloy. Comp. 509 (2011) 1607–1614.
[17] S. Huang, W. Li, X. Li, S. Schönecker, L. Bergqvist, E. Holmström, L.K. Varga, L. Vitos, Mechanism of magnetic transition in FeCrCoNi-based high entropy alloys, Mater. Des. 103 (2016) 71–74.
[18] M.S. Lucas, D. Belyea, C. Bauer, N. Bryant, E. Michel, Z. Turgut, S.O. Leontsev, J. Horwath, S.L. Semiatin, M.E. McHenry, C.W. Miller, Thermomagnetic analysis of FeCoCrxNi alloys: magnetic entropy of high-entropy alloys, J. Appl. Phys. 113 (2013) 17A923.
[19] M.S. Lucas, L. Mauger, J.A. Muñoz, Y. Xiao, A.O. Sheets, S.L. Semiatin, J. Horwath, Z. Turgut, Magnetic and vibrational properties of high-entropy alloys, J. Appl. Phys. 109 (2011) 07E307.
[20] C. Niu, A.J. Zaddach, A.A. Oni, X. Sang, J.W. Hurt, J.M. LeBeau, C.C. Koch, D.L. Irving, Spin-driven ordering of Cr in the equiatomic high entropy alloy NiFeCrCo, Appl. Phys. Lett. 106 (2015) 161906.
[21] H.P. Chou, Y.S. Chang, S.K. Chen, J.W. Yeh, Microstructure, thermophysical and electrical properties in AlxCoCrFeNi ($0 \le x \le 2$) high-entropy alloys, Mater. Sci. Eng., B 163 (2009) 184–189.
[22] Y.F. Kao, T.J. Chen, S.K. Chen, J.W. Yeh, Microstructure and mechanical property of as-cast, -homogenized, and -deformed AlxCoCrFeNi ($0 \le x \le 2$) high-entropy alloys, J. Alloy. Comp. 488 (2009) 57–64.
[23] W.R. Wang, W.L. Wang, S.C. Wang, Y.C. Tsai, C.H. Lai, J.W. Yeh, Effects of Al addition on the microstructure and mechanical property of AlxCoCrFeNi high-entropy alloys, Intermetallics 26 (2012) 44–51.
[24] K. Sato, L. Bergqvist, J. Kudrnovský, P.H. Dederichs, O. Eriksson, I. Turek, B. Sanyal, G. Bouzerar, H. Katayama-Yoshida, V.A. Dinh, T. Fukushima, H. Kizaki, R. Zeller, First-principles theory of dilute magnetic semiconductors, Rev. Mod. Phys. 82 (2010) 1633–1690.
[25] L. Bergqvist, O. Eriksson, J. Kudrnovský, V. Drchal, P. Korzhavyi, I. Turek, Magnetic percolation in diluted magnetic semiconductors, Phys. Rev. Lett. 93 (2004) 137202.
[26] F. Körmann, D. Ma, D.D. Belyea, M.S. Lucas, C.W. Miller, B. Grabowski, M.H.F. Sluiter, "Treasure maps" for magnetic high-entropy-alloys from theory and experiment, Appl. Phys. Lett. 107 (2015) 142404.
[27] L. Vitos, Total-energy method based on the exact muffin-tin orbitals theory, Phys. Rev. B 64 (2001) 014107.
[28] L. Vitos, Computational Quantum Mechanics for Materials Engineers, Springer, London, 2007.
[29] P. Soven, Coherent-potential model of substitutional disordered alloys, Phys. Rev. 156 (1967) 809–813.
[30] B.L. Győrffy, Coherent-potential approximation for a nonoverlapping-muffin-tin-potential model of random substitutional alloys, Phys. Rev. B 5 (1972) 2382–2384.
[31] L. Vitos, I.A. Abrikosov, B. Johansson, Anisotropic lattice distortions in random alloys from first-principles theory, Phys. Rev. Lett. 87 (2001) 156401.
[32] J.P. Perdew, K. Burke, M. Ernzerhof, Generalized gradient approximation made simple, Phys. Rev. Lett. 77 (1996) 3865–3868.
[33] B.L. Győrffy, A.J. Pindor, J. Staunton, G.M. Stocks, H. Winter, A first-principles theory of ferromagnetic phase transitions in metals, J. Phys. F Met. Phys. 15 (1985) 1337–1386.
[34] J.W. Yeh, S.Y. Chang, Y.D. Hong, S.K. Chen, S.J. Lin, Anomalous decrease in X-ray diffraction intensities of Cu–Ni–Al–Co–Cr–Fe–Si alloy systems with multi-principal elements, Mater. Chem. Phys. 103 (2007) 41–46.
[35] Z. Wu, H. Bei, F. Otto, G.M. Pharr, E.P. George, Recovery, recrystallization, grain growth and phase stability of a family of FCC-structured multi-component equiatomic solid solution alloys, Intermetallics 46 (2014) 131–140.
[36] B.C. Sales, K. Jin, H. Bei, G.M. Stocks, G.D. Samolyuk, A.F. May, M.A. McGuire, Quantum critical behavior in a concentrated ternary solid solution, Sci. Rep. 6 (2016) 26179.
[37] T.T. Zuo, R.B. Li, X.J. Ren, Y. Zhang, Effects of Al and Si addition on the structure and properties of CoFeNi equal atomic ratio alloy, J. Magn. Magn Mater. 371 (2014) 60–68.
[38] K. Jin, S. Mu, K. An, W.D. Porter, G.D. Samolyuk, G.M. Stocks, H. Bei, Thermophysical properties of Ni-containing single-phase concentrated solid solution alloys, Mater. Des. 117 (2017) 185–192.
[39] J. Guo, X. Huang, W. Huang, Microstructure and room-temperature mechanical properties of FeCrMoVTix high-entropy alloys, J. Mater. Eng. Perform. 26 (2017) 3071–3078.
[40] T. Zuo, M.C. Gao, L. Ouyang, X. Yang, Y. Cheng, R. Feng, S. Chen, P.K. Liaw, J.A. Hawk, Y. Zhang, Tailoring magnetic behavior of CoFeMnNiX (X = Al, Cr, Ga, and Sn) high entropy alloys by metal doping, Acta Mater. 130 (2017) 10–18.
[41] L. Liu, J.B. Zhu, C. Zhang, J.C. Li, Q. Jiang, Microstructure and the properties of FeCoCuNiSnx high entropy alloys, Mater. Sci. Eng. A 548 (2012) 64–68.
[42] S. Jiang, D. Sun, Y. Zhang, S. Wang, C. Zhao, Plastic deformation mechanisms of equiatomic $Ni_{20}Ti_{20}Fe_{20}Al_{20}Cu_{20}$ high-entropy alloy at high temperatures, J. Mater. Sci. 52 (2017) 3199–3207.
[43] A. Marshal, K.G. Pradeep, D. Music, S. Zaefferer, P.S. De, J.M. Schneider, Combinatorial synthesis of high entropy alloys: introduction of a novel, single phase, body-centered-cubic FeMnCoCrAl solid solution, J. Alloy. Comp. 691 (2017) 683–689.
[44] C. Li, J.C. Li, M. Zhao, Q. Jiang, Effect of alloying elements on microstructure and properties of multiprincipal elements high-entropy alloys, J. Alloy. Comp. 475 (2009) 752–757.
[45] Y.X. Zhuang, W.J. Liu, Z.Y. Chen, H.D. Xue, J.C. He, Effect of elemental interaction on microstructure and mechanical properties of FeCoNiCuAl alloys, Mater. Sci. Eng. A 556 (2012) 395–399.
[46] K.B. Zhang, Z.Y. Fu, J.Y. Zhang, W.M. Wang, H. Wang, Y.C. Wang, Q.J. Zhang, J. Shi, Microstructure and mechanical properties of CoCrFeNiTiAlx high-entropy alloys, Mater. Sci. Eng. A 508 (2009) 214–219.
[47] F. Otto, Y. Yang, H. Bei, E.P. George, Relative effects of enthalpy and entropy on the phase stability of equiatomic high-entropy alloys, Acta Mater. 61 (2013) 2628–2638.
[48] Y. Zhang, Y.J. Zhou, J.P. Lin, G.L. Chen, P.K. Liaw, Solid-solution phase formation rules for multi-component alloys, Adv. Eng. Mater. 10 (2008) 534–538.
[49] G. Laplanche, P. Gadaud, O. Horst, F. Otto, G. Eggeler, E.P. George, Temperature dependencies of the elastic moduli and thermal expansion coefficient of an equiatomic, single-phase CoCrFeMnNi high-entropy alloy, J. Alloy. Comp. 623 (2015) 348–353.
[50] D. Ma, B. Grabowski, F. Körmann, J. Neugebauer, D. Raabe, Ab initio thermodynamics of the CoCrFeMnNi high entropy alloy: importance of entropy contributions beyond the configurational one, Acta Mater. 100 (2015) 90–97.
[51] X.F. Wang, Y. Zhang, Y. Qiao, G.L. Chen, Novel microstructure and properties of multicomponent CoCrCuFeNiTix alloys, Intermetallics 15 (2007) 357–362.
[52] M. Kurniawan, A. Perrin, P. Xu, V. Keylin, M. McHenry, Curie temperature engineering in high entropy alloys for magnetocaloric applications, IEEE Magn. Lett. 7 (2016) 1–5.
[53] B. Cantor, I.T.H. Chang, P. Knight, A.J.B. Vincent, Microstructural development in equiatomic multicomponent alloys, Mater. Sci. Eng. A 375–377 (2004) 213–218.
[54] S. Guo, C.T. Liu, Phase stability in high entropy alloys: formation of solid-solution phase or amorphous phase, Prog. Nat. Sci. Mater. Int 21 (2011) 433–446.
[55] S. Huang, Á. Vida, D. Molnár, K. Kádas, L.K. Varga, E. Holmström, L. Vitos, Phase stability and magnetic behavior of FeCrCoNiGe high-entropy alloy, Appl. Phys. Lett. 107 (2015) 251906.
[56] O. Schneeweiss, M. Friák, M. Dudová, D. Holec, M. Šob, D. Kriegner, V. Holý, P. Beran, E.P. George, J. Neugebauer, A. Dlouhý, Magnetic properties of the CrMnFeCoNi high-entropy alloy, Phys. Rev. B 96 (2017) 014437.
[57] W. Ji, W. Wang, H. Wang, J. Zhang, Y. Wang, F. Zhang, Z. Fu, Alloying behavior and novel properties of CoCrFeNiMn high-entropy alloy fabricated by mechanical alloying and spark plasma sintering, Intermetallics 56 (2015) 24–27.
[58] B. Skubic, J. Hellsvik, L. Nordström, O. Eriksson, A method for atomistic spin dynamics simulations: implementation and examples, J. Phys. Condens. Matter 20 (2008) 315203.
[59] O.N. Senkov, J.D. Miller, D.B. Miracle, C. Woodward, Accelerated exploration of multi-principal element alloys with solid solution phases, Nat. Commun. 6 (2015) 6529.
[60] K.A. Gschneidner, Physical properties and interrelationships of metallic and semimetallic elements, Solid State Phys. 16 (1964) 275–426.